Available online at www.sciencedirect.com
ScienceDirect
Ceramics International 36 (2010) 87–91
CERAMICS INTERNATIONAL
www.elsevier.com/locate/ceramint

The properties of Al-doped TiO_2 nanoceramic films deposited by simultaneous rf and dc magnetron sputtering

Su-Shia Lin [a,*], Ding-Kun Wu [b]

[a] Department of Applied Materials and Optoelectronic Engineering, National Chi Nan University, Puli, Nantou Hsien 54561, Taiwan, ROC
[b] Department of Electrical Engineering, National Chi Nan University, Puli, Nantou Hsien 54561, Taiwan, ROC

Received 18 March 2009; received in revised form 29 May 2009; accepted 30 June 2009
Available online 16 July 2009

Abstract

The Al-doped TiO_2 (TiO_2:Al) nanoceramic films were deposited by simultaneous rf magnetron sputtering of TiO_2 and dc magnetron sputtering of Al. The advantage of this method is that the Al content could be independently controlled. Al_2O_3 was favorable to form with decreasing Al content. The nanocrystallinity was enhanced by increasing the Al contents, because the increase of Al contents resulted in that the deposited films to be nearly stoichiometric. The morphologies of TiO_2:Al films were significantly affected by Al contents. The nonlinear refractive index of TiO_2:Al film on the glass substrate was measured by Moiré deflectometry, and was of the order of 10^{-8} cm^2 W^{-1}. As Al content increased, the TiO_2:Al film had high VIS-IR transmission, high optical energy gap, high linear refractive index and low porosity.

Keywords: Films; Sputtering; Transmission; Refractive index

1. Introduction

Titanium dioxide (TiO_2) thin films are extensively studied because of their interesting chemical, electrical and optical properties (high band gap, transparent in the visible range, high refractive index, high dielectric constant, and ability to be easily doped with active ions) which are considered for various optical applications such as high refractive index component of multilayer optical filter, gas sensors, antireflective coating, photocatalysts, planar waveguides [1–3]. TiO_2 thin films have been prepared by several techniques, including chemical vapor deposition [4], aerosol pyrolysis [5], electrodeposition [6], sol–gel process [7], evaporation [8] and various sputtering methods [9,10].

Several dopants, such as Ce and W [11], Cu [12], Nb and Cr [13], and Pt [14], have been used to dope TiO_2. Few studies of Al-doped TiO_2 (TiO_2:Al) films have been reported. In this study, TiO_2:Al nanoceramic films were prepared by simultaneous rf magnetron sputtering of TiO_2 and dc magnetron sputtering of Al. The advantages of sputtering are the simplicity of the apparatus, high deposition rate, low substrate temperature, good surface flatness, and high density of the deposited layer [15]. The Al content was controlled by dc power. The Al content how to affect the properties of TiO_2:Al films was investigated.

Transparent materials generally exhibit the optical Kerr effect. The nonlinear refractive indices of materials are of great interest because of their potential applications in designing optical devices and laser technology [16–19]. Moiré deflectometry is a powerful tool for measuring the nonlinear refractive indices of materials. The main advantages of the Moiré deflectometry technique are its extreme experimental simplicity, lower cost and lower sensitivity to external disturbances than other interferometric methods. In this study, this method is applied to measure the nonlinear refractive indices of TiO_2:Al films on glass substrates under illumination with a 5-mW He–Ne laser ($\lambda = 632.8$ nm).

2. Experimental procedures

The TiO_2:Al nanoceramic films were deposited on glass (Corning 1737) by simultaneous rf magnetron sputtering of TiO_2 and dc magnetron sputtering of Al. The dimension of the glass substrates was 24 mm × 24 mm × 1.1 mm. Before

* Corresponding author. Tel.: +886 49 2910960x4771; fax: +886 49 2912238.
E-mail address: sushia@ncnu.edu.tw (S.-S. Lin).

0272-8842/$36.00
doi:10.1016/j.ceramint.2009.06.023

deposition, the substrates were ultrasonically cleaned in alcohol, rinsed in deionized water and dried in nitrogen. Two circular targets were used (5 cm diameter, 5 mm thickness); the first was sintered stoichiometric TiO_2 (99.99% purity); the other was metallic Al (99.999% purity).

The sputtering was performed in an Ar atmosphere with a target-to-substrate distance of 15 cm. A turbo-molecular pump, backed by a rotary pump, was used to achieve a base pressure of 1.3×10^{-4} Pa. For the deposition of the films, the substrates were not heated. The working pressure was 1.5 Pa. An rf power (13.56 MHz, RGN CONTROLLER, ULVAC, Japan) of 50 W was supplied to the TiO_2 target, and a dc power (DCS0052B, ULVAC, Japan) of 0–6 W was applied to the Al target. No external bias voltage was applied to substrate. The rotating speed of the substrate was 20 rpm, and the thickness of films was in the range of 20–120 nm.

The film thickness was measured using a surface profiler (Alpha-Step 500, TENCOR, Santa Clara, CA). X-ray diffraction (XRD; Rigaku D/MAX2500, Japan) was used to study the crystal structure. The elemental compositions were investigated by X-ray photoemission spectroscopy (XPS; PHI 5000 VersaProbe, Japan). The surface morphologies and surface roughness were examined by atomic force microscopy (AFM; Agilent 5500, Santa Clara, CA). The optical transmission spectra of films in the visible-infrared (VIS-IR) region were obtained using a spectrophotometer (HP 8452A diode array spectrophotometer, Hewlett Packard, Palo Alto, CA). The linear refractive indices of films were recorded using a spectrometer (MP100-ST, Fremont, CA).

Fig. 1 shows the Moiré deflectometry experimental set-up that is used to measure the nonlinear refractive indices of TiO_2:Al films on glass substrates. Lens L_1 focused a 5-mW He–Ne laser beam (wavelength of 632.8 nm), which was re-collimated by lens L_2. The focal lengths of lenses L_1, L_2 and L_3 were 100, 200 and 200 mm, respectively. Two similar Ranchi gratings G_1 and G_2 with a pitch of 0.1 mm were used to construct the Moiré fringe patterns. The distance between the planes of G_1 and G_2 was set to 64 mm, which is one of the Talbot distances of the used gratings. The Talbot distances satisfy $z_t = tp^2/\lambda$ where p is the periodicity of the grating; λ is the wavelength of light; t is an integer. In this work, the Moiré fringes were clearly formed for a Talbot distance of $z_{t=4} \approx 64$ mm, indicating that the Moiré fringes were observed on a screen attached to the second grating. The Moiré fringe patterns were projected onto a computerized CCD camera by lens L_3, which was placed at the back of the second grating.

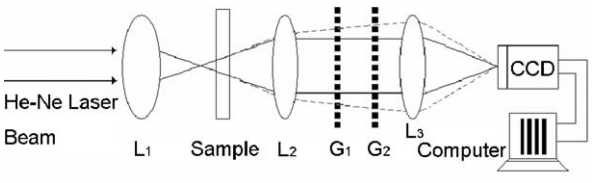

Fig. 1. The experimental set-up for measuring index of nonlinear refraction by Moiré deflectometry technique.

Table 1
Elemental composition of the TiO_2:Al films, deposited at different dc powers, obtained by XPS.

dc power (W)	O content (at.%)	Ti content (at.%)	Al content (at.%)	O/(Ti + Al)
0	60.1	39.9	0	1.51
4	62.7	35.6	1.7	1.68
6	63.1	34.4	2.5	1.71
8	63.3	32.9	3.8	1.72

3. Results and discussion

3.1. Structural characterization

Table 1 shows the results of elemental composition analysis of TiO_2:Al films deposited at different dc powers detected by XPS. The Al content of the sputtered films increased with the dc power to the Al target, whereas the Ti content decreased. The O/(Ti + Al) atomic ratio increased with Al content, suggesting that the deposited films became more stoichiometric when Al content increased.

Fig. 2 shows the X-ray diffraction patterns of TiO_2:Al films with different Al contents. XRD analysis was conducted on the films using a Rigaku D/MAX2500 goniometer with 18 kW rotating anode X-ray, equipped with a thin film attachment unit. The equipment was operated with Cu Kα ($\lambda = 1.5418$ Å) radiation at 40 kV, 100 mA and a scanning speed of 4° min^{-1} at an incident angle of 3°. The interval of the scan was 0.01° and the scanning range was 10–80°. From Fig. 2, it can be found that there is a broad diffraction peak (1 0 1) corresponding to nanocrystalline anatase TiO_2 film. Nanocrystalline rutile and anatase could be obtained also with low temperature synthesis; the crystallization and transformation temperatures have a great variability and strongly depend from a large number of parameters [20].

Compared with TiO_2, TiO_2:Al film showed the stronger peak (1 0 1) and the location of the measured diffraction peak shifted towards the lower diffraction angle as Al was doped. It

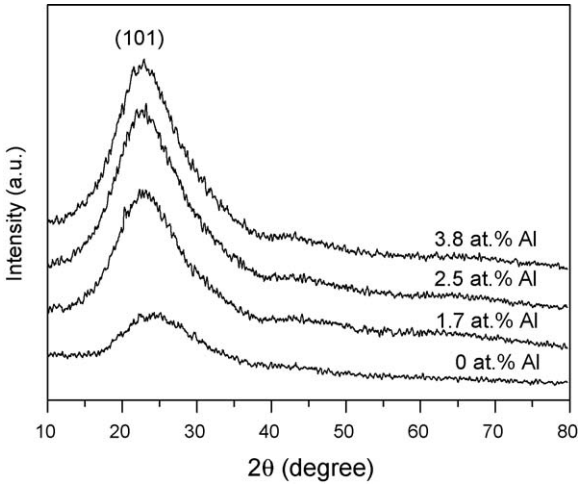

Fig. 2. The X-ray diffraction patterns of TiO_2:Al films with different Al contents.

indicated that the nanocrystallite of TiO_2 film was changed by Al atoms substituting in the Ti sites [21]. Bachari et al. [22] reported that the oxygen deficiency leaded to the growth of less homogeneous films with more crystallographic faults, and a decrease in the long-range order in the deposited films. It suggested that the non-stoichiometric films displayed poor crystallinity. Similarly, TiO_2 films showed stronger peaks (1 0 1) due to more stoichiometric when Al content increased. It indicated that the nanocrystallinity was enhanced as Al content increased.

The bonding condition of aluminum on the surface of TiO_2:Al films were investigated by XPS spectra. Fig. 3 shows Al 2p photoelectron peak in the XPS spectrum of TiO_2:Al films with Al contents of (a) 2.5 at.% and (b) 3.8 at.%. In Fig. 3a, the Al 2p peak at 74.3 eV was due to the aluminum in aluminum oxide [23]. It indicated that most Al atoms were as the substitutional atoms in the lattice of TiO_2 nanocrystallites in the film. In Fig. 3b, the major peak (A) at 74.3 eV was thought to be due to the aluminum in aluminum oxide and the shoulder peak (B) at 72.7 eV was due to metallic aluminum [23]. The shoulder peak (B) was due to metallic aluminum present, as interstitial atoms in the lattice of TiO_2 nanocrystallites in the film.

Fig. 4 shows the morphologies of TiO_2:Al films with different Al contents. The root-mean-square (RMS) roughness decreased from 0.5244 to 0.2805 nm when the Al content increased from 0 to 1.7 at.%. However, the roughness increased with the further increase in the Al content. The roughness values were very close to the morphologies of growing films [24]. The isolated columnar structures were formed as TiO_2:Al films with Al content of 3.8 at.%. It was probably due to metallic aluminum present, as interstitial atoms in the lattice of TiO_2 nanocrystallites in the film. It is a result of the nonequilibrium growth.

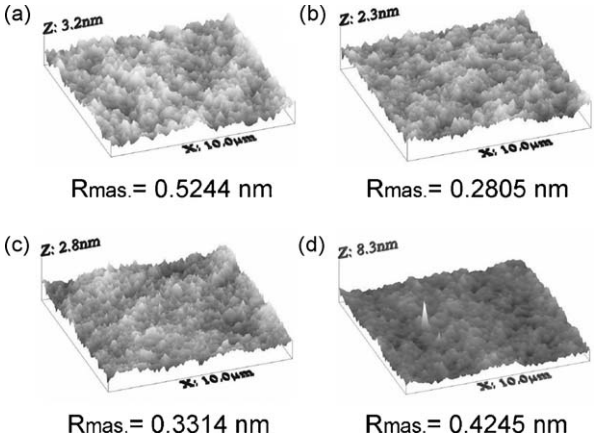

Fig. 4. The morphologies of TiO_2:Al films with Al contents of (a) 0 at.%; (b) 1.7 at.%; (c) 2.5 at.% and (d) 3.8 at.%.

3.2. Optical characterization

The optical energy gap E_g could be obtained from the intercept of $(\alpha h\nu)^2$ versus $h\nu$ for direct allowed transitions [25]. Better linearity was observed for $(\alpha h\nu)^2$ versus $h\nu$ [25,26] as shown in Fig. 5. The values of E_g were 2.65 eV and 2.7 eV for the films with Al contents of 0 at.% and 1.7 at.%. Obviously, Al-doped TiO_2 film had higher optical energy gap than TiO_2 film. Similar results have been reported previously by Sernelius et al. [27] and Hamberg et al. [28] who studied the optical properties of Al-doped ZnO films and Sn-doped In_2O_3 films.

Fig. 6 shows the transmission in the VIS-IR region of (a) TiO_2:Al films with different Al contents and (b) TiO_2:Al films with 1.7 at.% Al prepared at different thickness. In Fig. 6a, the transmission of TiO_2 films could be improved by doping with Al.

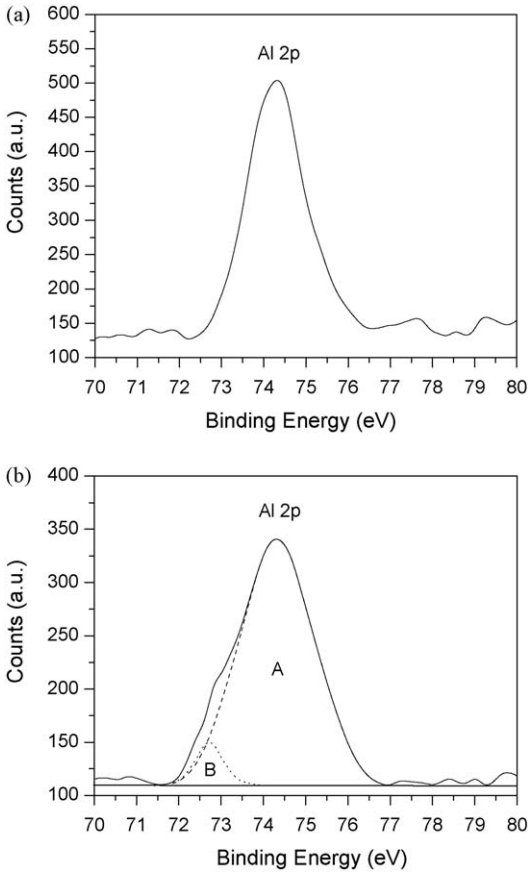

Fig. 3. Al 2p photoelectron peak in the XPS spectrum of TiO_2:Al films with Al contents of (a) 2.5 at.% and (b) 3.8 at.%.

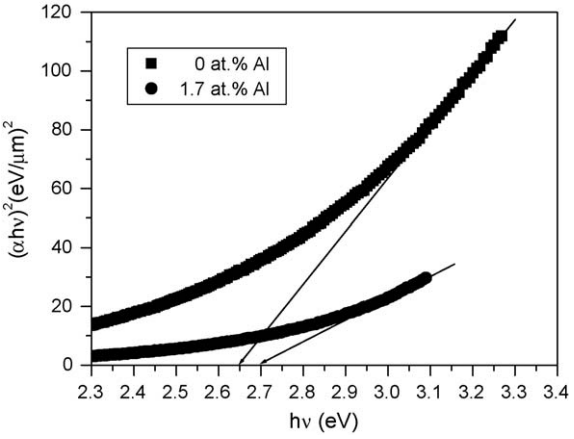

Fig. 5. Plots of $(\alpha h\nu)^2$ vs. $h\nu$ for TiO_2:Al films with different Al contents.

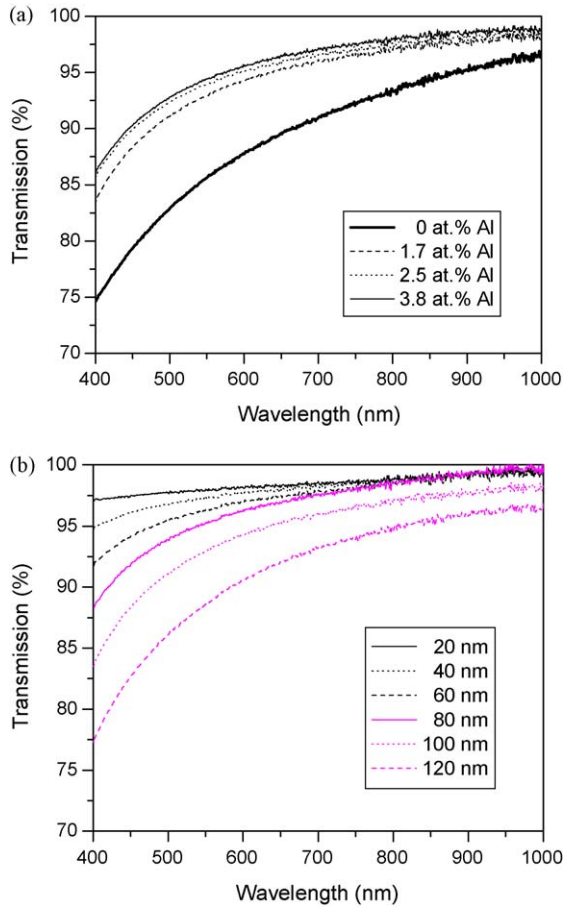

Fig. 6. The transmission in the VIS-IR region of (a) TiO_2:Al films with different Al contents and (b) TiO_2:Al films with 1.7 at.% Al prepared at different thickness.

It was probably due to the relatively low surface roughness, which could result in less light scattering [29]. As the Al content increased to 3.8 at.%, the transmission of TiO_2:Al films increased, but not by much. These results indicate that Al contents affect the transmission of films significantly. Furthermore, the transmission in the visible region increased obviously with the decrease of film thickness as shown in Fig. 6b.

The index of refraction, n, which depends on the radiation intensity, may be expressed in terms of the nonlinear index n_2 ($cm^2\ W^{-1}$):

$$n(r,z) = n_0 + n_2 I(r,z) = n_0 + \Delta n(r,z) \tag{1}$$

where n_0 is the linear index of refraction, $I(r, z)$ is the irradiance of the laser beam within the sample, and $\Delta n(r, z)$ is the light-induced change in refractive index. Based on the assumption that a Gaussian beam is traveling in the $+z$ direction, the beam irradiance can be written as

$$I(r,z) = I_0 \frac{\omega_0^2}{\omega^2(z)} \exp\left[-\frac{2r^2}{\omega^2(z)}\right] \tag{2}$$

where r is the radial radius of the imaginary sphere; ω_0 is the spot size of the beam at the focus; $\omega(z) = \omega_0(1 + z^2/z_0^2)^{1/2}$ is the beam radius at a distance z from the position of the waist; $z_0 = \pi\omega_0^2/\lambda$ is the diffraction length of the Gaussian beam, and λ is the wavelength. The irradiance of the beam at the focus is denoted I_0 and in terms of the input laser power, p_{in}, equals $2p_{in}/\pi\omega_0^2$. Therefore, for a Gaussian laser beam, the radial dependence of the irradiance gives rise to a radially dependent parabolic refractive index change near the beam axis:

$$\Delta n(r,z) = n_2 I_0 \frac{\omega_0^2}{\omega^2(z)} \exp\left[-\frac{2r^2}{\omega^2(z)}\right] \tag{3}$$

Moiré deflectometry is a sensitive technique for measuring changes in the refractive indices of materials. The sensitivity of this technique is determined by the minimum measurable angle of rotation (α_{min}). Fig. 7 shows the Moiré fringe rotation angle versus z for the TiO_2:Al film with 1.7 at.% Al on the glass substrate. The tested sample was placed at various distances from the focal point of lens L_1. The minimum angle of rotation was obtained from the figure. The same experiment was performed using only a pure glass substrate to check the contribution of the glass substrate to the nonlinear refraction measurement. No observed fringe rotation or change in fringe size was found.

For the thin nonlinear medium of thickness d, the lowest nonlinear refractive index can be written as

$$n_{2,min} = \frac{\theta f_2^2}{z_t} \frac{\pi\omega_0^4}{d\, p_{in} z_0^2} \alpha_{min} \tag{4}$$

and the change in the minimum refractive index is

$$\Delta n_{min} = \frac{\omega_0^2 \theta f_2^2}{2 d z_t z_0^2} \alpha_{min} \tag{5}$$

Fig. 8 shows the minimum nonlinear refractive index and the change in the minimum refractive index of TiO_2:Al film with 1.7 at.% Al prepared at different thickness on glass substrate. The nonlinear refraction index was measured to be of the order of $10^{-8}\ cm^2\ W^{-1}$ and the change in refractive index was of the order of 10^{-5}.

Fig. 9 shows the linear refractive index and the porosity of TiO_2:Al films with different Al contents. The linear refractive index n_0 was measured at a wavelength of 632.8 nm. The linear

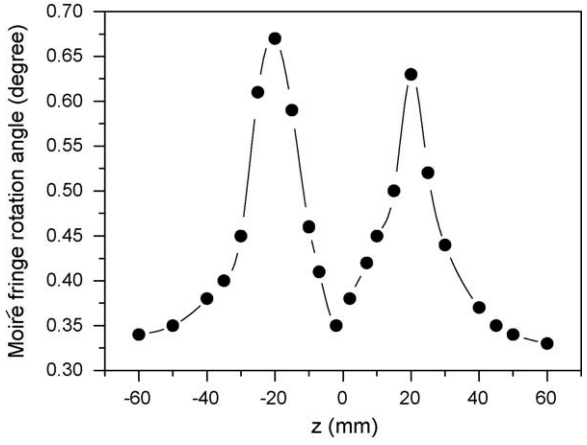

Fig. 7. The Moiré fringe rotation angle versus z for the TiO_2:Al film with 1.7 at.% Al on the glass substrate.

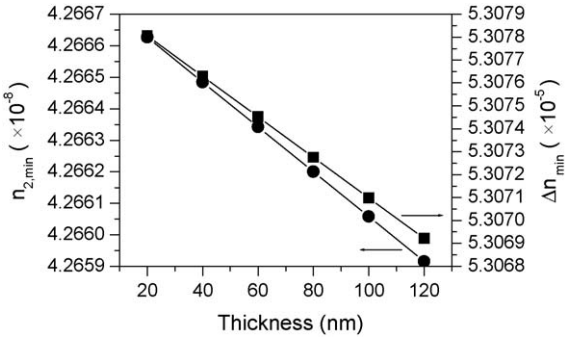

Fig. 8. The minimum nonlinear refractive index and the change in the minimum refractive index of TiO_2:Al film with 1.7 at.% Al prepared at different thickness on glass substrate.

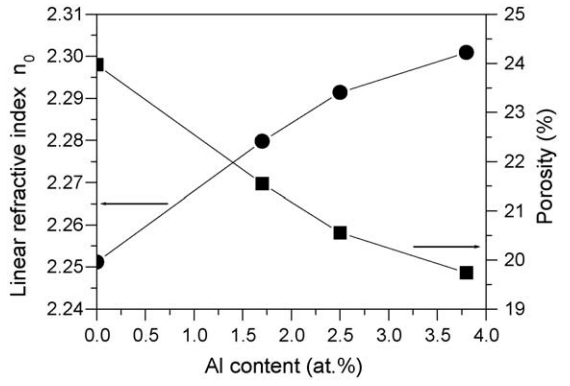

Fig. 9. The linear refractive index and the porosity of TiO_2:Al films with different Al contents.

refractive index of TiO_2:Al film increased with the Al content. The linear refractive index was found to correlate with the porosity [30]. In this study, all the deposited films are assumed to be homogeneous. The porosity of the thin films can be calculated using the following equation [31]:

$$\text{Porosity}(\%) = \left(1 - \frac{n_0^2 - 1}{n_a^2 - 1}\right) \times 100 \quad (6)$$

where n_0 is the linear refractive index of the porous thin film and n_a is the linear refractive index of pore-free anatase ($n_a = 2.52$) found in the literature [32]. The porosity of the TiO_2:Al film decreased as the Al content increased.

4. Conclusions

The Al contents of TiO_2:Al films were controlled by the dc power applied to the Al target. Al_2O_3 was more favorable to form as Al content was decreased. The TiO_2:Al film had a similar structure to that of the TiO_2 film and corresponded to nanocrystalline anatase. The increase of Al content enhanced the nanocrystallinity of TiO_2:Al film. The morphologies of films were significantly affected by the Al contents. With increasing Al contents, the films had higher optical energy gap and VIS-IR transmission. The nonlinear refraction index of the TiO_2:Al film on the glass substrate was measured to be of the order of 10^{-8} cm^2 W^{-1} and the change in the refractive index was of the order of 10^{-5}. As the Al content increased, the linear refractive index of the TiO_2:Al film increased, but the porosity decreased.

Acknowledgements

The authors would like to thank the National Science Council of the Republic of China, Taiwan, for financially supporting this research under Contract No. NSC-97-2221-E-260-004.

References

[1] D.P. Partlow, T.W. O'Keeffe, Appl. Opt. 29 (10) (1990) 1526.
[2] A. Brunik, H. Cztemastek, K. Zakrzewska, M. Jachimowski, Thin Solid Films 199 (1) (1991) 45.
[3] L. Yang, S. Scott Saavedra, N.R. Armstrong, J. Hayes, Anal. Chem. 66 (8) (1994) 1254.
[4] Y. Guo, X.W. Zhang, G.R. Han, Mater. Sci. Eng. B 135 (2006) 83.
[5] L. Kavan, M. Grätzel, Electrochem. Acta 40 (1995) 643.
[6] Y. Lei, L.D. Zhang, J.C. Fan, Chem. Phys. Lett. 338 (2001) 231.
[7] W. Que, A. Uddin, X. Hu, J. Power Sources 159 (2006) 353.
[8] L. Sun, P. Hou, Thin Solid Films 455–456 (2004) 525.
[9] S.F. Wang, Y.F. Hsu, Y.S. Lee, Ceram. Int. 32 (2006) 121.
[10] X. He, X. Zhao, B. Liu, J. Non-Cryst. Solids 354 (2008) 1267.
[11] L. Zheng, Sens. Actuators B 94 (2003) 294.
[12] N.O. Savage, S.A. Akbar, P.K. Dutta, Sens. Actuators B 72 (2001) 239.
[13] K. Zakrzewska, Vacuum 74 (2004) 335.
[14] J. Trimboli, P.K. Dutta, Sens. Actuators B 102 (2004) 132.
[15] K.H. Yoon, J.W. Choi, D.H. Lee, Thin Solid Films 302 (1997) 116.
[16] M.J. Soileau, W.E. Williams, N. Mansour, E.W. Van Stryland, Opt. Eng. 28 (1989) 1133.
[17] E.W. Van Stryland, Y.Y. Wu, D.J. Hagan, M.J. Soileau, K. Mansour, J. Opt. Soc. Am. B 5 (1988).
[18] M.J. Soileau, W.E. Williams, E.W. Van Stryland, IEEE J. Q. Electr. QE-19 (1983) 731.
[19] K. Mansour, M.J. Soileau, E.W. Van Stryland, J. Opt. Soc. Am. B 3 (1992) 1100.
[20] Y. Djaoued, S. Badilescu, P.V. Ashrit, D. Bersani, P.P. Lottici, R. Bruening, J. Sol–Gel Sci. Technol. 24 (2002) 247.
[21] S.S. Lin, J.L. Huang, P. Šajgalik, Surf. Coat. Technol. 191 (2–3) (2005) 286.
[22] E.M. Bachari, G. Baud, S. Ben Amor, M. Jacquet, Thin Solid Films 348 (1999) 165.
[23] C.D. Wagner, W.M. Riggs, L.E. Davis, J.F. Moulder, G.E. Muilenberg, Handbook of X-ray Photoelectron Spectroscopy, Perkin-Elmer Corporation, Eden Prairie, MN, 1979, pp. 50–51.
[24] G. Laukaitis, S. Lindroos, S. Tamulevičius, M. Leskelä, Appl. Surf. Sci. 185 (2001) 134.
[25] N. Serpone, D. Lawless, R. Khairutdinov, J. Phys. Chem. 99 (1995) 16646.
[26] D. Di Claudio, A.R. Phani, S. Santucci, Opt. Mater. 30 (2007) 279.
[27] B.E. Sernelius, K.F. Berggren, Z.C. Jin, I. Hamberg, C.G. Granqvist, Phys. Rev. B 37 (1988) 10244.
[28] I. Hamberg, C.G. Granqvist, K.F. Berggren, B.E. Sernelius, L. Engström, Phys. Rev. B 30 (1984) 3240.
[29] T. Yamamoto, T. Shiosaki, A. Kawabata, J. Appl. Phys. 51 (6) (1980) 3113.
[30] G.S. Vicente, A. Morales, M.T. Gutierrez, Thin Solid Films 391 (2001) 133.
[31] B.E. Yoldas, P.W. Partlow, Thin Solid Films 129 (1985) 1.
[32] W.D. Kingery, H.K. Bowen, D.R. Uhlmann, Introduction to Ceramics, Wiley, New York, 1976, p. 669.